Optimal robust control of vehicle lateral stability using damped least-square backpropagation training of neural networks

Taghavifar, H., Hu, C., Taghavifar, L., Qin, Y., Na, J. & Wei, C.

Original citation & hyperlink:
Taghavifar, H, Hu, C, Taghavifar, L, Qin, Y, Na, J & Wei, C 2020, 'Optimal robust control of vehicle lateral stability using damped least-square backpropagation training of neural networks', Neurocomputing, vol. 384, pp. 256-267.
https://dx.doi.org/10.1016/j.neucom.2019.12.045

DOI 10.1016/j.neucom.2019.12.045
ISSN 0925-2312

Publisher: Elsevier

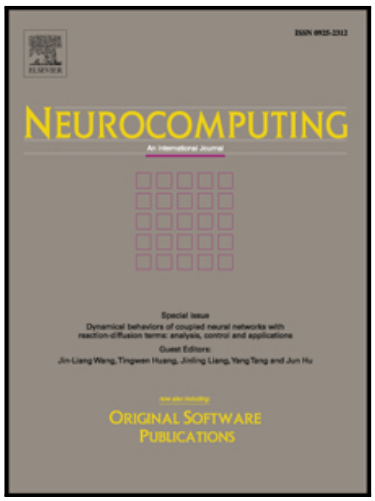

Optimal Robust Control of Vehicle Lateral Stability using Damped Least-Square Backpropagation training of Neural Networks

Hamid Taghavifar , Chuan Hu , Leyla Taghavifar , Yechen Qin , Jing Na , Chongfeng Wei

PII: S0925-2312(19)31754-0
DOI: https://doi.org/10.1016/j.neucom.2019.12.045
Reference: NEUCOM 21674

To appear in: *Neurocomputing*

Received date: 23 July 2019
Revised date: 25 October 2019
Accepted date: 10 December 2019

Please cite this article as: Hamid Taghavifar , Chuan Hu , Leyla Taghavifar , Yechen Qin , Jing Na , Chongfeng Wei , Optimal Robust Control of Vehicle Lateral Stability using Damped Least-Square Backpropagation training of Neural Networks, *Neurocomputing* (2019), doi: https://doi.org/10.1016/j.neucom.2019.12.045

Optimal Robust Control of Vehicle Lateral Stability using Damped Least-Square Backpropagation training of Neural Networks

Hamid Taghavifar[1], Chuan Hu[2], Leyla Taghavifar[3], Yechen Qin[4]*, Jing Na[5], Chongfeng Wei[6]

1 School of Mechanical, Aerospace and Automotive Engineering, Coventry University, Coventry, UK
2 Department of Mechanical Engineering University of Texas at Austin, Austin, TX, US
3 Department of Electrical and Electronics Engineering, Islamic Azad University, Tehran, Iran
4 School of Mechanical Engineering, Beijing Institute of Technology, Beijing, China, Corresponding author, qinyechenbit@gmail.com
5 Mechanical and Electrical Engineering, Kunming University of Science and Technology, Kunming, China
6 Institute of Transport Studies, University of Leeds, Leeds, U.K

Abstract—Chassis control systems play a significant role in achieving the desired vehicle performance and stability during various severe maneuvers. A probabilistic estimation approach by hybridization of optimal robust control and a damped least-square backpropagation based neural networks (NN) is proposed to design a control system for dealing with unknown nonlinear dynamics of a passenger car. To this end, a four-wheel active steering (4WAS) model is employed and a multilayer perceptron (ML) feed-forward backpropagation neural network (FFBPNN) model is developed as an approximator. The optimal robust control is employed to regulate the yaw rate and side-slip angle of the vehicle to follow the desired vehicle response. The developed FFBPNN model is trained to distinguish the nonlinear dynamics of the vehicle and the corresponding optimal feedback gain during a wide range of operating conditions via the state variables. The robustness of the controller is evaluated using Lyapunov stability method. The performance of the proposed controller is analyzed considering the open-loop and closed-loop responses of the nonlinear vehicle model and a sliding mode controller to track the desired yaw rate and side-slip angle responses. The results obtained during severe maneuvers suggest that the proposed control method can substantially enhance the handling and stability performances of the vehicle.

Keywords— Artificial Neural Networks, Damped Least-Square Backpropagation, Vehicle Control, Optimal Control.

I. INTRODUCTION

Active chassis control systems such as anti-lock braking system, four-wheel steering, and active front steering are several effective control methods to stabilize the vehicle performance and handling severe maneuvers [1-3]. The limited region of functionality related to each controlling scheme is the major bottleneck in the mass commercialization and employment of such active controllers [3]. The main objective of the active chassis controlling approach is to attain the real-time vehicle response close to the desired vehicle states obtained from the reference vehicle model by reducing the tracking errors. The vehicle lateral chassis control systems have demonstrated capabilities of enhanced shared steering control for cooperative automated driving [4], reducing single-vehicle accidents in order to increase the passenger safety [5], vehicle maneuverability and steering flexibility [6].

Various factors can deteriorate vehicle stability, such as the spontaneous change in road-tire grip, side wind force, tire inflation pressure and disturbance due to the steering input [7]. Therefore, it is essential to generate a sufficient yaw moment to compensate for any disturbance that the driver may not respond well. Four-wheel-steering (4WS) vehicles have revealed a substantial capacity to enhance the maneuverability of vehicles at low speed and improve the stability at high speed because rear wheels participate in the steering process and the transient response of a vehicle can be increased drastically [8].

On the other side, a direct yaw control (DYC) method can be used by generating an external yaw moment through a differential braking system in order to improve vehicle active safety [9]. For increasing the performance of such controllers, an integrated DYC and active front steering (AFS) methods are typically utilized [10-12], which can increase the power demand of the system. Furthermore, because DYC depends on regulating the tire longitudinal and lateral force differences in the left and right wheels rather than directly employing the tire lateral force, it may not be sufficient in controlling the side-slip angle.

There exists a bulk of studies related to the integrated active chassis control systems to improve the handling and stability of a vehicle under harsh driving conditions effectively. Zhang and Wang [12] employed a combined AFS/DYC control method for the enhancement of vehicle lateral stability and vehicle handling performance while the major concept was to employ a varying longitudinal velocity rather than a constant vehicle speed, which may typically impose the fore-aft discomfort for the passengers. In another time-varying velocity based vehicle lateral dynamics stabilization problem, a robust gain-scheduling state-feedback controller by an energy-to-peak control of DYC for stabilizing lateral motion of electric vehicles was proposed in [13]. Although the proposed linear matrix inequality (LMI) based controlling method was shown to present robustness to parametric uncertainties, it may not be sufficiently effective in the region of tire nonlinearities. Li *et al.*, [14] proposed a three-dimensional dynamic stability controller considering the effect of time delay on vehicle stability control. The potential of an integrated stability control related to the yaw and yaw-roll stabilities and rollover prevention was evaluated by using an upper and a lower controller. The framework showed effectiveness in achieving lateral stability and rollover prevention. The discussed integrated AFS/DYC methods, however, typically display extra power demand and potential inefficiency in controlling the side-slip angle which serves as a critical state parameter to reach the desired vehicle performance.

The performance of drive-by-wire systems has also been explored for integrated motion control [15,16]. Song *et al.*, [15] designed a multiple hierarchical layers system for the purpose of integrated chassis controller of full drive-by-wire vehicles. Two control methods of sliding mode control (SMC) and terminal SMC were used for vehicle motion control purposes. It was shown that the method could satisfactorily deal with the constraints of the tire adhesive by employing polygonal simplification method. Abe and Mokhiamar [16], proposed an integrated vehicle motion control for a full drive-by-wire vehicle in order to control the steering angles and torques of the wheels independently. However, these methods depend on

optimum tire force distribution rather than directly dealing with the tire lateral force and may thus offer undesired performance for high-speed maneuvers.

In view of control methods, a broad range of techniques have been applied for the active chassis control problems such as fractional order [17], Adaptive Neuro-Fuzzy Inference System (ANFIS) [18], Fuzzy Logic Control (FLC) [19,20], optimal control [11, 21], and SMC [5,15,16]. Reinforcement learning-based adaptive optimal exponential algorithms, resilient adaptive H_∞ have also demonstrated satisfactory performance for tracking control systems with unknown dynamics, actuator faults, and actuator nonlinearities [21-23]. An integrated system for controlling the nonlinear vehicle system was proposed based on ANFIS and Fractional-order $PI^{\lambda}D^{\mu}$ control algorithms, respectively, while the multibody vehicle dynamic response was considered [18]. The model was designed to control the yaw velocity and side-slip angle while the control rules and membership functions of fuzzy control rules were updated by of ANFIS, and the parameters of Fractional-order $PI^{\lambda}D^{\mu}$ control were adjusted using genetic algorithm (GA) optimization. Li and Fu [24] designed an FLC to enhance vehicle performance for the integrated 4WS and active braking system. The two inputs of FLC were the yaw rate error and side-slip angle error while the outputs were the yaw moment and rear steering angle. Type-1 Takagi-Sugeno and Mamdani fuzzy systems however exhibit low robustness to uncertainties, although interval type-2 fuzzy systems can potentially address this challenge by fuzzy definition of membership functions [25]. Esmailzadeh *et al.* [26] investigated the ability of two optimal and semi-optimal controllers to generate yaw moment through traction forces on two sides of the vehicle for an electric vehicle. It was reported that the optimal controller is suggestive of improved performance when compared to the semi-optimal controller at high lateral accelerations at the expense of higher complexity as it requires both yaw rate and lateral velocity feedback. Similarly, hybrid multi-level optimal control solvers have shown effectiveness in enhancing the stability and narrow down the initial guess sensitivity for trajectory optimization and parking maneuvering of autonomous vehicles [27, 28]. Among the methods mentioned above, the optimal control strategy has demonstrated a reasonably good performance to deal with the linear time-invariant (LTI) systems. These control schemas, mainly linear quadratic regulator (LQR), are vulnerable when subject to disturbances and thereby cannot provide a reliable and satisfactory result particularly when the dynamical system is nonlinear. However, the capacity of artificial intelligence (AI) can be employed to estimates the feedback gain of the optimal control for a nonlinear vehicle model after a dynamic programming implementation to learn the time-variant dynamics of the system.

The reviewed literature indicates that 4WAS serves as an effective method to stabilize the vehicle lateral dynamics in terms of the desired yaw-rate and side-slip angle responses. However, further studies are required regarding the optimal controllers to deal with the nonlinear vehicle model while the feedback gains are generated under a wide range of vehicle operating conditions.

To this end, this paper spearheads training an optimized neural network (NN) model to learn the nonlinear vehicle dynamic model and estimate the optimal feedback gains for the controller using a damped leas-square backpropagation algorithm while the robustness of the system is guaranteed through Lyapunov stability method. Subsequently, the output of the optimized NN model as the feedback gain is updated progressively based on any disturbance to the system, such as the front steering angle or wind force. The dynamically updating feedback estimator for the nonlinear vehicle model will be evaluated for different steering inputs compared to the classical SMC method.

II. Problem Formulation

In order to control a vehicle to follow the desired yaw rate and side-slip angle, it is essential to develop a mathematical model that includes the vehicle lateral dynamics and identifies the relationship between the

vehicle and the road. In this section, the nonlinear tire model, together with the vehicle dynamic model and a linear vehicle model as the model reference are described.

A. Nonlinear tire model

The Burckhardt tire model [29] is employed with combined longitudinal and lateral slip in order to describe the tire longitudinal and lateral forces as it is particularly suitable for analytical purposes while retaining a good degree of accuracy in the description of the friction coefficient [30]. The longitudinal and lateral tire forces are expressed as a function of the longitudinal slip and side-slip as well as the vertical force applied to the wheels as follows.

$$[F_{xj} \quad F_{yj}] = f(s_{qj}, F_{zj}, s_{pj}) \quad j = 1,2,3,4 \qquad (1)$$

Burckhardt method is one of the models, which illustrates different longitudinal and lateral tire forces. It is valid for a wide range of road surfaces, together with the validity in the nonlinear region of the tire.

B. Vehicle Dynamics model

The vehicle considered in this paper is a mid-sized vehicle with four independent drive wheels. The model includes the longitudinal and lateral forces in the yaw plane obtained from nonlinear tire model based on Burckhardt technique [29]. It is assumed that the contribution of the pitch and roll modes of motion on the lateral dynamics of the vehicle are infinitesimal due to the symmetricity of the car about the right- and left-side tracks. Additionally, the longitudinal dynamics of the vehicle are ignored by assuming the constant speed cornering of the car. Moreover, the longitudinal dynamics of the car can be controlled independently. Therefore, the 2 degree-of-freedom (DOF) vehicle model is considered for the purpose of vehicle dynamics modeling as appreciated from Fig. 1 wherein the degrees of freedom include the vehicle yaw rate and side-slip angle. The governing equations of the 2-DOF model can be described as follows

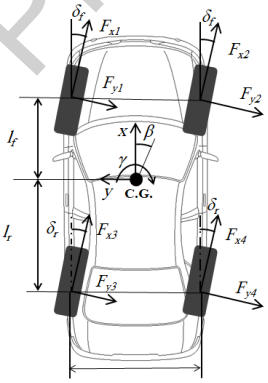

Fig. 1. Planar 2-DOF vehicle handling model

$$(F_{x1} + F_{x2})sin\delta_f + (F_{x3} + F_{x4})sin\delta_r + (F_{y1} + F_{y2})cos\delta_f + (F_{y3} + F_{y4})cos\delta_r = mv_x(\dot{\beta} + \gamma) \qquad (1)$$

$$[(F_{y1} + F_{y2})cos\delta_f + (F_{x1} + F_{x2})sin\delta_f]l_f - [(F_{y3} + F_{y4})cos\delta_r + (F_{x3} + F_{x4})sin\delta_r]l_r + \frac{w}{2}[(F_{x1} - F_{x2})cos\delta_f + (F_{x3} - F_{x4})cos\delta_r] - \frac{w}{2}[(F_{y1} - F_{y2})cos\delta_f + (F_{y3} - F_{y4})cos\delta_r] = I_{zz}\dot{\gamma} \qquad (2)$$

where m is the mass of vehicle, v_x stands for the longitudinal velocity of the vehicle center of gravity (*C.G.*), I_{zz} is the yaw moment of inertia, γ is the yaw rate, $F_{xj,}$ and F_{yj} (j = 1, ., 4) are the longitudinal forces and lateral forces respectively, developed by tire j (j = 1, ., 4), l_f and l_r are the distances from vehicle *C.G.* to the front and rear axles, respectively, w is the track width and δ_f and δ_r are the front and rear-wheel steering angles, respectively.

A Burckhardt method based nonlinear tire model was incorporated in the governing equations of motion (1) and (2), where the longitudinal force F_p and the lateral force F_q of the tires are described in terms of the longitudinal and lateral slip variables, respectively.

$$\begin{cases} F_{pj}(s_{pj}, v_{pj}) = [c_1(1 - e^{-c_2 s_{pj}}) - c_3 s_{pj}]e^{-c_4 s_{pj} v_{pj}} F_{zj} \\ F_{qj}(s_{qj}, v_{qj}) = [c_1(1 - e^{-c_2 s_{qj}}) - c_3 s_{qj}]e^{-c_4 s_{qj} v_{qj}} F_{zj} \end{cases} \quad j = 1, \dots, 4 \tag{3}$$

where F_z is the vertical load of the tires, $s_{pj}$and s_{qj} are the longitudinal and lateral slip, c_1, c_2, c_3, and c_4 are the model parameters of the tires obtained empirically depending on surface and tire interaction. The longitudinal and lateral slips can be obtained as follows.

$$s_{pj} = \begin{cases} \frac{R_w \omega_j - v_{pj}}{R_w \omega_j} & R_w \omega_j \geq v_{pj} \\ \frac{v_{pj} - R_w \omega_j}{R_w \omega_j} & R_w \omega_j \leq v_{pj} \end{cases} \quad j = 1,2,3,4 \tag{4}$$

$$s_{qj} = \begin{cases} \delta_j - \beta - \left(\frac{l_f \gamma}{v_x}\right) & j = 1,2 \\ \delta_j - \beta + \left(\frac{l_r \gamma}{v_x}\right) & j = 3,4 \end{cases} \tag{5}$$

where $R_w$denotes the wheel radius, δ is the steering angle of the wheel, β expresses the side-slip angle and ω and v_p are the wheel rotational and actual translational velocities, respectively. The longitudinal and lateral load transfers are ignored for the 2-DOF vehicle model, and the vertical loads on the front and rear tires are expressed by

$$\begin{cases} F_{zf} = \frac{l_r}{(l_f + l_r)} \frac{mg}{2} \\ F_{zf} = \frac{l_f}{(l_f + l_r)} \frac{mg}{2} \end{cases} \tag{6}$$

The resultant slip of the tires can be also described according to:

$$s_{Res} = \sqrt{{s_{pj}}^2 + {s_{qj}}^2} \qquad j = 1,2,3,4 \tag{7}$$

Therefore, (3) can be rewritten as:

$$\begin{cases} F_{pj} = \frac{s_{pj}[c_1(1 - e^{-c_2 s_{pj}}) - c_3 s_{pj}]e^{-c_4 s_{pj} v_{pj}}}{s_{Res}} F_{zj} \\ F_{qj} = \frac{s_{qj}[c_1(1 - e^{-c_2 s_{qj}}) - c_3 s_{qj}]e^{-c_4 s_{qj} v_{qj}}}{s_{Res}} F_{zj} \end{cases} \quad j = 1,2,3,4 \tag{8}$$

The tire forces estimated from the Burckhardt tire model are expressed in the wheel coordinate system. The tire forces are translated to the chassis-fixed coordinate system based on to their steering angle δ as following:

$$\begin{bmatrix} F_{xj} \\ F_{yj} \end{bmatrix} = \begin{bmatrix} \cos\delta_j & -\sin\delta_j \\ \sin\delta_j & \cos\delta_j \end{bmatrix} \begin{bmatrix} F_{pj} \\ F_{qj} \end{bmatrix} \quad j = 1,2,3,4 \tag{9}$$

where F_{xj} and F_{yj} are the vehicle-fixed coordinate forces in the *(x,y)* coordinate obtained from F_{pj} and F_{qj} tire forces.

C. Reference model

The reference model is developed by assuming the linear response of tires. The simplified model is obtained by attributing constant cornering stiffness values to the front and rear tires. The yaw rate is a direct function of the steering angle in the linearized vehicle handling state thereby the vehicle response can be estimated at any input steering angle. Accordingly, the constant cornering stiffness parameter multiplied by the side-slip angle estimates the lateral force through the Burckhardt model at zero longitudinal slip-ratio. Furthermore, the desired yaw rate is a function of front steering angle and vehicle forward speed while the desired body side-slip angle is considered at zero for the sake of simplicity. The 2-DOF linear reference model can be described in the state-space form as follows.

$$\dot{\boldsymbol{x}} = \boldsymbol{A}\boldsymbol{x} + \boldsymbol{B}\boldsymbol{u} \tag{10}$$

where

$$\boldsymbol{A}=\begin{bmatrix}\frac{c_{sr}-c_{sf}}{mv_x} & -1-\frac{l_fc_{sf}-l_rc_{sr}}{mv_x{}^2}\\ \frac{l_rc_{sr}-l_fc_{sf}}{I_{zz}} & -\frac{l_f{}^2c_{sf}+l_r{}^2c_{sr}}{I_{zz}v_x}\end{bmatrix},\ \boldsymbol{B}=\begin{bmatrix}\frac{c_{sf}}{mv_x} & \frac{c_{sr}}{mv_x}\\ \frac{l_fc_{sf}}{I_{zz}} & -\frac{l_rc_{sr}}{I_{zz}}\end{bmatrix},\ \boldsymbol{u}=\begin{bmatrix}\delta_f\\ \delta_r\end{bmatrix},\ \boldsymbol{x}=[\beta \quad \gamma]^T$$

The matrices of the state-space above are defined by the front and rear axle tire cornering stiffness values c_{sf} and c_{sr}. The minimum side-slip angle of the vehicle chassis, which is ideally zero, with the ideal yaw-rate response, which is obtained from the steady-state yaw response of the linearized vehicle model describes the objectives for the handling performance of the vehicle. In this manner, the desired side-slip angle and yaw-rate responses that a typical vehicle should follow during cornering maneuvers can be defined at zero and a function of the front steering wheel input, respectively [3].

$$\boldsymbol{x_{ref}}=\begin{cases}\beta_{ref}=0\\ \gamma_{ref}=\dfrac{\frac{v_x}{(l_f+l_r)}}{\frac{1+mv_x{}^2(l_fc_{sf}-l_rc_{sr})}{c_{sf}c_{sr}(l_f+l_r)^2}}\delta_f\end{cases} \tag{11}$$

Therefore, the control objective is to make the system states $\boldsymbol{x}$ in (10) converge to the reference values $\boldsymbol{x_{ref}}$ defined in (11) $\boldsymbol{x}\rightarrow\boldsymbol{x_{ref}}$. The developed controller for this system should efficiently deal with the disturbances basically created by the front steering input. There have been controllers that could effectively consider the uncertainties in the dynamic responses of the system, including different vehicle design parameters tire properties [3]. In the present paper, the controller is designed to provide the yaw moment and force through the rear steering-wheel angles in order to follow the desired trajectories. The inputs to the proposed optimal controller are the yaw rate error and the side-slip angle error while the designed controller is synthesized to perform reasonably well in the vehicle nonlinear operating region.

In order to describe the nonlinear vehicle dynamical model in a more general form (12), the cornering stiffness values of the tires are rephrased using the Burckhardt tire model in the chassis-fixed coordinates and are replaced instead of the constant linearized reference model.

$$\begin{aligned}\dot{\boldsymbol{x}}(\boldsymbol{t})&=\boldsymbol{f}\big(t,\boldsymbol{x}(t),\boldsymbol{u}(t)\big)\\ \boldsymbol{y}(\boldsymbol{t})&=\boldsymbol{h}\big(t,\boldsymbol{x}(t),\boldsymbol{u}(t)\big)\end{aligned} \tag{12}$$

Therefore, the variations of local forces of the tires obtained from Burckhardt model with respect to the side-slip angle are derived and the state-space form is rewritten [3].

$$\hat{C}_{sj}=\frac{\partial F_{yj}}{\partial\delta_j}=\frac{\partial F_{pj}}{\partial\delta_j}\sin\delta_j+\frac{\partial F_{qj}}{\partial\delta_j}\cos\delta_j+F_{pj}\cos\delta_j-F_{qj}\sin\delta_j \quad j=f,r \tag{13}$$

$$\begin{bmatrix}\dot{\beta}\\ \dot{\gamma}\end{bmatrix}=\underbrace{\begin{bmatrix}\frac{\hat{C}_{sr}-\hat{C}_{sf}}{mv_x} & -1-\frac{l_f\hat{C}_{sf}-l_r\hat{C}_{sr}}{mv_x{}^2}\\ \frac{l_r\hat{C}_{sr}-l_f\hat{C}_{sf}}{I_{zz}} & -\frac{l_f{}^2\hat{C}_{sf}+l_r{}^2\hat{C}_{sr}}{I_{zz}v_x}\end{bmatrix}}_{f(\boldsymbol{x})}\begin{bmatrix}\beta\\ \gamma\end{bmatrix}+\underbrace{\begin{bmatrix}\frac{\hat{C}_{sr}}{mv_x}\\ -\frac{l_r\hat{C}_{sr}}{I_{zz}}\end{bmatrix}}_{g(\boldsymbol{x})}\delta_r+\underbrace{\begin{bmatrix}\frac{\hat{C}_{sf}}{mv_x}\\ \frac{l_f\hat{C}_{sf}}{I_{zz}}\end{bmatrix}}_{o(\boldsymbol{x})}\delta_f \tag{14}$$

Finally, (14) can be stated in general form as following:

$$\dot{\boldsymbol{x}}(t)=f\big(t,\boldsymbol{x}(t)\big)+g\big(t,\boldsymbol{x}(t)\big)\boldsymbol{u}(t)+o\big(t,\boldsymbol{x}(t)\big)\delta_f \tag{15}$$

where the functions $f\big(t,\boldsymbol{x}(t)\big)$ and $g\big(t,\boldsymbol{x}(t)\big)$ defined in (14) are functions of the system parameters and $o\big(t,\boldsymbol{x}(t)\big)\delta_f$ is the disturbance term caused by the front steering-angle input.

III. Controller Design

A. Optimal Robust Controller

The cost index, related to the vehicle lateral stability problem, to be minimized can be written in general form of a cross-weighted cost:

$$J=\int_0^\infty(\tilde{\boldsymbol{x}}^T\boldsymbol{Q}\tilde{\boldsymbol{x}}+2\tilde{\boldsymbol{x}}^T\boldsymbol{N}\boldsymbol{u}+\boldsymbol{u}^T\boldsymbol{R}\boldsymbol{u})dt \tag{16}$$

Where $\tilde{\boldsymbol{x}} = \boldsymbol{x} - \boldsymbol{x}_{\boldsymbol{ref}}$, and the algebraic Riccati equation is defined [1]:

$$\boldsymbol{P}(\boldsymbol{A} - \boldsymbol{B}\boldsymbol{R}^{-1}\boldsymbol{N}^T) + (\boldsymbol{A} - \boldsymbol{B}\boldsymbol{R}^{-1}\boldsymbol{N}^T)^T\boldsymbol{P} - \boldsymbol{P}\boldsymbol{B}\boldsymbol{R}^{-1}\boldsymbol{B}^T\boldsymbol{P} + (\boldsymbol{Q} - \boldsymbol{N}\boldsymbol{R}^{-1}\boldsymbol{N}^T) = \boldsymbol{0} \quad (17)$$

where $\boldsymbol{Q}$ and $\boldsymbol{R}$ are positive-definite Hermitian matrices and $\boldsymbol{P} \in R^{n\times n}$ is a positive-definite matrix to satisfy the (17). If $\bar{\boldsymbol{P}}$ is the solution, the optimum gains obtained through:

$$\boldsymbol{K} = \boldsymbol{R}^{-1}(\boldsymbol{N}^T + \boldsymbol{B}^T\bar{\boldsymbol{P}}) \quad (18)$$

The transformation of the nonlinear vehicle dynamics model into the state-space through the neural network method is a key factor to identify the variable feedback gains by the increment of step size. The represented form of equations enables us to employ well-developed analysis and design methods. Nevertheless, if the knowledge about the system is inadequate, it is a difficult task to derive a representation with classical methods and thereby, an NN based approach is employed to define a state-space representation by means of the input-output data of the system. Regarding the state-space model presented in (12), one can also write that at any operating point $(\hat{x}_t, \hat{u}_t)$ for the state function $\boldsymbol{f}_x$:

$$\begin{aligned} \boldsymbol{f}_x(\boldsymbol{x},\boldsymbol{u}) &= \frac{\partial \boldsymbol{f}(\boldsymbol{x},\boldsymbol{u})}{\partial \boldsymbol{x}} \therefore \boldsymbol{A}_t \triangleq \boldsymbol{f}_x(\boldsymbol{x},\boldsymbol{u})\big|_{(\hat{x}_t,\hat{u}_t)} \\ \boldsymbol{f}_u(\boldsymbol{x},\boldsymbol{u}) &= \frac{\partial \boldsymbol{f}(\boldsymbol{x},\boldsymbol{u})}{\partial \boldsymbol{u}} \therefore \boldsymbol{B}_t \triangleq \boldsymbol{f}_u(\boldsymbol{x},\boldsymbol{u})\big|_{(\hat{x}_t,\hat{u}_t)} \end{aligned} \quad (19)$$

And similarly, for the same operating point for the output function $\boldsymbol{h}_x$, it can be stated that:

$$\begin{aligned} \boldsymbol{h}_x(\boldsymbol{x},\boldsymbol{u}) &= \frac{\partial \boldsymbol{h}(\boldsymbol{x},\boldsymbol{u})}{\partial \boldsymbol{x}} \therefore \boldsymbol{C}_t \triangleq \boldsymbol{h}_x(\boldsymbol{x},\boldsymbol{u})\big|_{(\hat{x}_t,\hat{u}_t)} \\ \boldsymbol{h}_x(\boldsymbol{x},\boldsymbol{u}) &= \frac{\partial \boldsymbol{h}(\boldsymbol{x},\boldsymbol{u})}{\partial \boldsymbol{u}} \therefore \boldsymbol{D}_t \triangleq \boldsymbol{h}_u(\boldsymbol{x},\boldsymbol{u})\big|_{(\hat{x}_t,\hat{u}_t)} \end{aligned} \quad (20)$$

the linearized state space equations are obtained as

$$\begin{aligned} \dot{\boldsymbol{x}}(t) &= \boldsymbol{A}_t\boldsymbol{x}(t) + \boldsymbol{B}_t\boldsymbol{u}(t) \\ \boldsymbol{y}(t) &= \boldsymbol{C}_t\boldsymbol{x}(t) + \boldsymbol{D}_t\boldsymbol{u}(t) \end{aligned} \quad (21)$$

Now it is possible to assign state-space matrices at any time step (t) and obtain the corresponding full-state feedback using the optimal control theory. Therefore, the feedback gains at any point is obtained considering (21) and its equivalent index function (16) with the solution to find the feedback gains so that the controller input is:

$$\boldsymbol{u}(t) = -\boldsymbol{K}\tilde{\boldsymbol{x}}(t) \quad (22)$$

Herein, we provide proof of stability for the developed optimal controller subject to disturbance and uncertainty as follows. One can consider a generic representation for the linear, time-variant system in state-space form as follows [1]:

$$\dot{\boldsymbol{x}}(t) = \boldsymbol{A}(t)\boldsymbol{x}(t) + \boldsymbol{B}(t)[\boldsymbol{u}(t) + \boldsymbol{d}(t)] \quad (23)$$

where $\boldsymbol{d}(t) \in R^m$ is the disturbance vector, and $\boldsymbol{A}(t)$ and $\boldsymbol{B}(t)$ are the time-variant matrices including the disturbance with appropriate dimensions such that:

$$\boldsymbol{A}(t) = \boldsymbol{A} + \Delta\boldsymbol{A}(t), \boldsymbol{B}(t) = \boldsymbol{B} + \Delta\boldsymbol{B}(t) \quad (24)$$

$$\Delta\boldsymbol{A}(t) = \boldsymbol{Q}_{\boldsymbol{A}}\psi(t)\boldsymbol{R}_{\boldsymbol{A}},\ \Delta\boldsymbol{B}(t) = \boldsymbol{Q}_{\boldsymbol{B}}\psi(t)\boldsymbol{R}_{\boldsymbol{B}} \quad (25)$$

where $\|\psi(t)\| \leq 1$ and $\boldsymbol{Q}_i, \boldsymbol{R}_i, i = \boldsymbol{A}, \boldsymbol{B}$ vectors with appropriate size such that (25) forms the disturbed terms in (24). According to the Pontryagin minimum principle, we can develop the minimum quadratic performance index in finite horizon and time interval $t \in [t_1, t_2]$ as follows:

$$I = \frac{1}{2}\left[\tilde{\boldsymbol{x}}^T(t_2)\boldsymbol{\Xi}(t_2)\tilde{\boldsymbol{x}}(t_2) + \int_{t_1}^{t_2} \tilde{\boldsymbol{x}}^T(t)\boldsymbol{Q}(t)\tilde{\boldsymbol{x}}(t) + \boldsymbol{u}^T(t)\boldsymbol{R}(t)\boldsymbol{u}(t)\right] \quad (26)$$

where $\boldsymbol{\Xi} \in R^{n\times n}$ is a symmetric positive definite matrix, the disturbance is considered norm-bounded and $\boldsymbol{u}(t)$ is designed as expressed in (26).

$$\boldsymbol{u}(t) = -\boldsymbol{R}^{-1}(t)\boldsymbol{B}^T(t)\boldsymbol{P}(t)\tilde{\boldsymbol{x}}(t) \quad (27)$$

Owing to the time-invariant matrices in (23), the matrix differential Riccati equation can be developed as follows:

$$\dot{\boldsymbol{P}}(t) = -\boldsymbol{A}^T(t)\boldsymbol{P}(t) + \boldsymbol{P}(t)\boldsymbol{A}(t) + \boldsymbol{P}(t)\boldsymbol{B}(t)\boldsymbol{R}^{-1}(t)\boldsymbol{B}^T(t)\boldsymbol{P}(t) - \boldsymbol{Q}(t) \quad (28)$$

A Lyapunov function can be selected such as (29).

$$V = \tilde{\boldsymbol{x}}^T(t)\boldsymbol{P}(t)\tilde{\boldsymbol{x}}(t) \quad (29)$$

The time derivative of (29) yields:

$$\dot{V} = \dot{\tilde{\boldsymbol{x}}}^T(t)\boldsymbol{P}(t)\tilde{\boldsymbol{x}}(t) + \tilde{\boldsymbol{x}}^T(t)\dot{\boldsymbol{P}}(t)\tilde{\boldsymbol{x}}(t) + \tilde{\boldsymbol{x}}^T(t)\boldsymbol{P}(t)\dot{\tilde{\boldsymbol{x}}}(t) \tag{30}$$

By plugging (23) in (30) we get:

$$\dot{V} = \left[\left(\boldsymbol{A} + \Delta\boldsymbol{A}(t)\right)\tilde{\boldsymbol{x}}(t) + \left(\boldsymbol{B} + \Delta\boldsymbol{B}(t)\right)\left(\boldsymbol{u}(t) + \boldsymbol{d}(t)\right)\right]^T \boldsymbol{P}(t)\tilde{\boldsymbol{x}}(t) + \tilde{\boldsymbol{x}}^T(t)\dot{\boldsymbol{P}}(t)\tilde{\boldsymbol{x}}(t) + \tilde{\boldsymbol{x}}^T(t)\boldsymbol{P}(t)\left[\left(\boldsymbol{A} + \Delta\boldsymbol{A}(t)\right)\tilde{\boldsymbol{x}}(t) + \left(\boldsymbol{B} + \Delta\boldsymbol{B}(t)\right)\left(\boldsymbol{u}(t) + \boldsymbol{d}(t)\right)\right] \tag{31}$$

Considering that (31) is composed of two nominal and disturbed components, and that substituting (28) in (30), a component of (31) related to the nominal terms can be described as:

$$\dot{V}_1 = \left[\boldsymbol{A}\tilde{\boldsymbol{x}}(t) + \boldsymbol{B}\left(\boldsymbol{u}(t) + \boldsymbol{d}(t)\right)\right]^T \boldsymbol{P}(t)\tilde{\boldsymbol{x}}(t) + \tilde{\boldsymbol{x}}^T(t)[-\boldsymbol{A}^T(t)\boldsymbol{P}(t) + \boldsymbol{P}(t)\boldsymbol{A}(t) + \boldsymbol{P}(t)\boldsymbol{B}(t)\boldsymbol{R}^{-1}(t)\boldsymbol{B}^T(t)\boldsymbol{P}(t) - \boldsymbol{Q}(t)]\tilde{\boldsymbol{x}}(t) + \tilde{\boldsymbol{x}}^T(t)\boldsymbol{P}(t)\left[\boldsymbol{A}\tilde{\boldsymbol{x}}(t) + \boldsymbol{B}\left(\boldsymbol{u}(t) + \boldsymbol{d}(t)\right)\right] \tag{32}$$

Considering an algebraic manipulation, (32) can be shown by the semi-negative function (33):

$$\dot{V}_1 = -\tilde{\boldsymbol{x}}^T\boldsymbol{Q}\tilde{\boldsymbol{x}} - (\boldsymbol{B}^T\boldsymbol{P}\tilde{\boldsymbol{x}})^T\boldsymbol{R}^{-1}(\boldsymbol{B}^T\boldsymbol{P}\tilde{\boldsymbol{x}}) \leq 0 \tag{33}$$

One should note that the only condition $\dot{V}_1 = 0 \Leftrightarrow \tilde{\boldsymbol{x}} = \boldsymbol{0}$. The perturbed side of (30) can also be developed as:

$$\dot{V}_2 = \left[(\boldsymbol{Q_A}\psi(t)\boldsymbol{R_A})\tilde{\boldsymbol{x}}(t) + (\boldsymbol{Q_B}\psi(t)\boldsymbol{R_B})\left(\boldsymbol{u}(t) + \boldsymbol{d}(t)\right)\right]^T \boldsymbol{P}(t)\tilde{\boldsymbol{x}}(t) + \tilde{\boldsymbol{x}}^T(t)\boldsymbol{P}(t)\left[(\boldsymbol{Q_A}\psi(t)\boldsymbol{R_A})\tilde{\boldsymbol{x}}(t) + (\boldsymbol{Q_B}\psi(t)\boldsymbol{R_B})\left(\boldsymbol{u}(t) + \boldsymbol{d}(t)\right)\right] \tag{34}$$

Lemma 1 [31]: For any matrices (or vectors) Π and Λ with appropriate dimensions, one can write:

$$\boldsymbol{\Lambda}\psi(t)\boldsymbol{\Pi} + (\boldsymbol{\Lambda}\psi(t)\boldsymbol{\Pi})^T \leq \boldsymbol{\varepsilon}\boldsymbol{\Lambda}\boldsymbol{\Lambda}^T + \varepsilon^{-1}\boldsymbol{\Pi}\boldsymbol{\Pi}^T \tag{35}$$

where $\psi(t)^T\psi(t) \leq I$ and $\boldsymbol{\varepsilon} > 0$ are valid above.

Considering *Lemma 1,* the time varying uncertain terms of (31) can be bounded using arbitrary $\boldsymbol{\varepsilon} > 0$, it can be shown that:

$$\dot{V}_2 \leq \left[\underbrace{\tilde{\boldsymbol{x}}^T(t)\boldsymbol{R}^T{}_{\boldsymbol{A}}}_{\Lambda_1}\psi(t)\underbrace{\boldsymbol{Q}^T{}_{\boldsymbol{A}}\boldsymbol{P}(t)\tilde{\boldsymbol{x}}(t)}_{\Pi_1} + \underbrace{(\tilde{\boldsymbol{x}}^T(t)\boldsymbol{P}(t)\boldsymbol{Q_A}\psi(t)\boldsymbol{R_A})\tilde{\boldsymbol{x}}(t)}_{(\Lambda_1\psi(t)\Pi_1)^T}\right] + \left[\underbrace{\left(\boldsymbol{u^T}(t) + \boldsymbol{d^T}(t)\right)\boldsymbol{R}^T{}_{\boldsymbol{B}}}_{\Lambda_2}\psi(t)\underbrace{\boldsymbol{Q}^T{}_{\boldsymbol{B}}\boldsymbol{P}(t)\tilde{\boldsymbol{x}}(t)}_{\Pi_2} + \underbrace{\tilde{\boldsymbol{x}}^T(t)\boldsymbol{P}(t)\boldsymbol{Q_B}\psi(t)\boldsymbol{R_B}\left(\boldsymbol{u}(t) + \boldsymbol{d}(t)\right)}_{(\Lambda_2\psi(t)\Pi_2)^T}\right] - \varepsilon_1\tilde{\boldsymbol{x}}^T(t)\boldsymbol{R}^T{}_{\boldsymbol{A}}\boldsymbol{R_A}\tilde{\boldsymbol{x}}(t) + \varepsilon_1{}^{-1}\boldsymbol{Q}^T{}_{\boldsymbol{A}}\boldsymbol{P}(t)\tilde{\boldsymbol{x}}(t)\tilde{\boldsymbol{x}}^T(t)\boldsymbol{P}(t)\boldsymbol{Q_A} - \varepsilon_2\left(\boldsymbol{u^T}(t) + \boldsymbol{d^T}(t)\right)\boldsymbol{R}^T{}_{\boldsymbol{B}}\boldsymbol{R_B}\left(\boldsymbol{u}(t) + \boldsymbol{d}(t)\right) + \varepsilon_2{}^{-1}\boldsymbol{Q}^T{}_{\boldsymbol{B}}\boldsymbol{P}(t)\tilde{\boldsymbol{x}}(t)\tilde{\boldsymbol{x}}^T(t)\boldsymbol{P}(t)\boldsymbol{Q_B} = 0 \tag{36}$$

From (33) and (36) it can be safely concluded that $\dot{V} = \dot{V}_1 + \dot{V}_2 \leq 0$, and this completes the proof. ■

B. Neural Network Design

The main objective of the design of the neural network (NN) system here is to estimate the optimal robust feedback gains (Fig. 2). Therefore, the inputs to the NN are the states of the vehicle model $\boldsymbol{x} = [\boldsymbol{x}_1 \quad \boldsymbol{x}_2 \cdots \boldsymbol{x}_R]^T$ multiplied by the corresponding synaptic weights $\boldsymbol{w} = [\boldsymbol{w}_{1h} \quad \boldsymbol{w}_{2h} \cdots \boldsymbol{w}_{Rh}]$ element-wise where $w_{jh} \in R$. The total input to an individual unit h is simply the weighted sum of the separate outputs from each of the connected units plus an offset term θ_{jh}.

$$s_h{}^R = \sum_{j=1}^{R} \boldsymbol{w}_{jh}\,\boldsymbol{x}_j + \theta_{jh} = \boldsymbol{w}\boldsymbol{x} + \boldsymbol{\theta_h} \tag{37}$$

And the transfer function passes the net input of the above neuron through the following *tangent-sigmoid* function:

$$\Theta(s_h{}^R) = \frac{2}{1+e^{-2s_h{}^R}} - 1 \tag{38}$$

The increased units, so-called hidden layers, from one to $q \mid \mathrm{q} \in \mathrm{N} - \{0\}$, forms the multilayer perceptron neural network as follows.

$$p^q = \Theta^q\left(\boldsymbol{w}^q\Theta^{q-1}\left(\boldsymbol{w}^{q-1}\Theta^{q-2}\cdots\left(\boldsymbol{w}^2\Theta^1\left(\boldsymbol{wy}+\boldsymbol{\theta_h}^1\right)+\boldsymbol{\theta_h}^2\right)\cdots+\boldsymbol{\theta_h}^{q-1}\right)\boldsymbol{\theta_h}^q\right) \tag{39}$$

The outputs of the perceptron in (39) are equivalent to the controller feedback gains ($\boldsymbol{K}$). It is inferred that the output of each neuron in the first layer is fed into the neurons in the subsequent layer and so forth. The complexity and nonlinearity of inputs, together with data size are suggestive of the increased layers at the expense of potential over-fitting drawbacks. Therefore, a single hidden layer was employed in the present study.

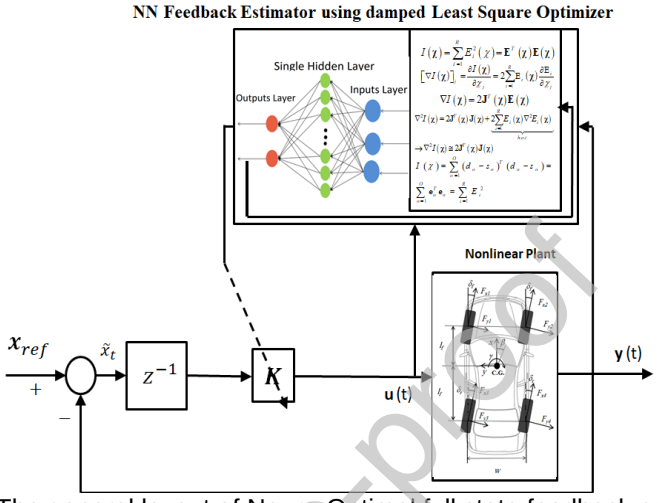

Fig. 2. The general layout of Neuro-Optimal full state feedback controller

The total quadratic error at the output units is designated as the error measure:

$$E^R = \frac{1}{2}\sum_R (d^R - {s_h}^R)^2 \tag{40}$$

Where $d^R$and ${s_h}^R$ represent the desired and actual AORC feedback gain values, respectively. The cost function above that represents the squared error between the desired feedback gains of the optimal controller and the ones predicted by the developed neural model is applied to the gradient descent method by finding the weights that minimize the error function as follows:

$$\Delta_R w_{jh} = -\gamma \frac{\partial E^R}{\partial w_{jh}} \tag{41}$$

where γ is the learning rate and (42) can be written using a chain rule:

$$\frac{\partial E^R}{\partial w_{jh}} = \frac{\partial E^R}{\partial {s_h}^R} \times \frac{\partial {s_h}^R}{\partial w_{jh}} \tag{42}$$

By plugging (37) in (42):

$$\frac{\partial {s_h}^R}{\partial w_{jh}} = {x_j}^R \tag{43}$$

And by defining

$$\frac{\partial E^R}{\partial {s_h}^R} = -{\lambda_h}^R \tag{44}$$

The updating rule that functions as gradient descent on the error surface is thereby created as following:

$$\Delta_R w_{jh} = \gamma {\lambda_h}^R {x_j}^R \tag{45}$$

However, the optimization method in the present study is the damped least-squares by interpolation of the above gradient descent and Gauss–Newton algorithm that fits well for the nonlinear least-squares problems and to avoid to trap in the local minima rather than the global solution, which typical gradient descent algorithms exhibit.

If we assume that $I(\boldsymbol{\chi})$ is a sum of squared function:

$$I(\boldsymbol{\chi}) = \sum_{i=1}^{R} E_i(\chi)^2 = \boldsymbol{E}^T(\boldsymbol{\chi})\boldsymbol{E}(\boldsymbol{\chi}) \tag{46}$$

Then the j_{th} element of the gradient would be

$$[\nabla I(\boldsymbol{\chi})]_j = \frac{\partial I(\boldsymbol{\chi})}{\partial \chi_j} = 2\sum_{i=1}^{R} E_i(\chi)\frac{\partial E_i(\chi)}{\partial \chi_j} \tag{47}$$

The gradient can, therefore, be written in matrix form:

$$\nabla I(\boldsymbol{\chi}) = 2\boldsymbol{J}^T(\boldsymbol{\chi})\boldsymbol{E}(\boldsymbol{\chi}) \tag{48}$$

where $\boldsymbol{J}(\boldsymbol{\chi})$ is the Jacobian matrix, however, the Newtonian method is proportional to the second order gradient of the sum of square function, thus the Hessian matrix can be presented as:

$$\nabla^2 I(\boldsymbol{\chi}) = 2\boldsymbol{J}^T(\boldsymbol{\chi})\boldsymbol{E}(\boldsymbol{\chi}) + \underbrace{2\sum_{i=1}^{R} E_i(\boldsymbol{\chi})\nabla^2 E_i(\boldsymbol{\chi})}_{h.o.t} \cong 2\boldsymbol{J}^T(\boldsymbol{\chi})\boldsymbol{E}(\boldsymbol{\chi}) \tag{49}$$

where the higher-order term is considered to be negligible, and thus the cost function for multilayer network training is the mean squared error (40), (46) can be rewritten as following for the *O* targets in the training set:

$$I(\boldsymbol{\chi}) = \sum_{o=1}^{O}(d_o - s_o)^T(d_o - s_o) = \sum_{o=1}^{O}(\boldsymbol{e}_o)^T(\boldsymbol{e}_o) = \sum_{i=1}^{R} {E_i}^2 \tag{50}$$

where d_o and s_o are the desired and predicted output using the neural representation. The critical task in the damped least-square minimization is to obtain the Jacobian matrix as well as the pseudo-inverse of the matrix while the damping factor plays a substantial role to avoid the singularities in the optimization problem. In order to implement such computation in the neural model, the derivatives of the errors were computed instead of the derivatives of the squared errors.

$$\boldsymbol{J}(\boldsymbol{\chi}) = \begin{bmatrix} \frac{\partial E_1(\boldsymbol{\chi})}{\partial \chi_1} & \frac{\partial E_1(\boldsymbol{\chi})}{\partial \chi_2} & \frac{\partial E_1(\boldsymbol{\chi})}{\partial \chi_3} \cdots \frac{\partial E_1(\boldsymbol{\chi})}{\partial \chi_R} \\ \frac{\partial E_2(\boldsymbol{\chi})}{\partial \chi_1} & \frac{\partial E_2(\boldsymbol{\chi})}{\partial \chi_2} & \frac{\partial E_2(\boldsymbol{\chi})}{\partial \chi_3} \cdots \frac{\partial E_2(\boldsymbol{\chi})}{\partial \chi_R} \\ \frac{\partial E_3(\boldsymbol{\chi})}{\partial \chi_1} & \frac{\partial E_3(\boldsymbol{\chi})}{\partial \chi_2} & \frac{\partial E_3(\boldsymbol{\chi})}{\partial \chi_3} \cdots \frac{\partial E_3(\boldsymbol{\chi})}{\partial \chi_R} \\ & & \vdots \\ \frac{\partial E_R(\boldsymbol{\chi})}{\partial \chi_1} & \frac{\partial E_R(\boldsymbol{\chi})}{\partial \chi_2} & \frac{\partial E_R(\boldsymbol{\chi})}{\partial \chi_3} \cdots \frac{\partial E_R(\boldsymbol{\chi})}{\partial \chi_R} \end{bmatrix} \tag{51}$$

where the error and input vectors can be defined as the following:

$$\begin{aligned} \boldsymbol{E} &= [E_1 \quad E_2 \quad E_3 \quad \cdots \quad E_R]^T \\ \boldsymbol{\chi} &= [\boldsymbol{w} \quad \boldsymbol{\theta_h}]^T \end{aligned} \tag{52}$$

By plugging (52) in (51), the Jacobian matrix for the multilayer network learning is developed and by considering the backpropagation method as:

$$\frac{\partial I(\boldsymbol{\chi})}{\partial \chi_j} = \frac{\partial \boldsymbol{e_o}^T \boldsymbol{e_o}}{\partial \chi_j} \tag{53}$$

For the elements of the Jacobian matrix that are needed for the damped least-square algorithm, we need to calculate the terms such as

$$[J]_{R,j} = \frac{\partial E_i(\chi)}{\partial \chi_j} \tag{54}$$

Moreover, considering the variables *n* and layer *m* and using a chain rule, derivation of backpropagation is obtained where the right-hand term is the sensitivity:

$$\frac{\partial I}{\partial w_{R,h}} = \frac{\partial I}{\partial n_R^m} \times \frac{\partial n_R^m}{\partial w_{R,h}} \tag{55}$$

The backpropagation process calculates the sensitivities by a recurrence relation for the sensitivity by using the chain rule in matrix form.

$$c_R^m \equiv \frac{\partial \boldsymbol{I}}{\partial n_R^m} = \frac{\partial \boldsymbol{E}}{\partial n_R^m} \therefore [J]_{R,j} \triangleq \frac{\partial E_i(\chi)}{\partial \chi_j} = \frac{\partial I}{\partial n_R^m} \times \frac{\partial n_R^m}{\partial w_{R,h}} = c_R^m \times \frac{\partial n_R^m}{\partial w_{R,h}} \tag{56}$$

During the backpropagation, the sensitivities can be computed through the same recurrence relations as the standard sensitivities [32].

The NN architecture is formulated considering the data obtained from the state-space model of the system and employing a reasonably large range of operating conditions generating a total of 2×10000 data

size. Considering the dynamics of the system, two outputs are identified and thereby two corresponding feedback gains are obtained optimally using the feedback gains at any step increment. The NN observer is then employed to learn the correct feedback gains required to track the desired response given any running point of the simulation. The first and second elements of the feedback vector correspond to the yaw rate and side-slip angle variables.

The proposed multilayer perceptron algorithm among the class of feed-forward networks has the capability of universal approximation of nonlinear phenomena and complex systems, therefore, the multilayer feed-forward neural network with damped least-square optimization method was employed. The designed neural network architecture consists of one input layer comprising both of the state variables, namely the yaw rate and side-slip angle. The single hidden layer is chosen due to the large size of the data and complex dependence of the feedback gains with those of state variables.

The challenging tasks for developing ANN models are to identify an optimal number of neurons in each hidden layer, number of hidden layers, training algorithms, transfer functions, and tuning of learning rate and momentum. Determination of an optimal number of hidden layers generally involves a difficult tradeoff between the prediction ability and computational demand of the model. The preliminary simulations performed with the proposed NN model with a single hidden layer revealed reasonably well estimations of the feedback gains over the entire range of adopted inputs. The designed neural network with a single hidden layer with neurons ranging from 1 to 20 was subsequently employed, which showed satisfactory convergence in terms of mean squared error (MSE). It is noteworthy that employing a greater number of neurons in each hidden layer may lead to the over-fitting drawback, which reduces the forecasting ability of the model [33]. The neurons within the selected range did not exhibit over-fitting, ensured smooth learning of the ANN model and provided reasonably good correlations between the predicted and measured responses during the cross-validation phase.

The network selects the weights and biases in a random manner at the start of the training phase, which not only entails greater computational demands but also may not yield satisfactory model performance. In order to overcome this drawback, each structure was trained 50 times to minimize the effect of random adoptions of weights and biases. Although increasing the number of repetitions may result in convergence toward zero MSE, it will impose excessive computational demands. The preliminary simulations revealed that the convergence towards minimal MSE could be realized within 1000 iterations. Subsequently, the network structure with least MSE over 100 iterations was explored. To ensure that each input variable provides an equal contribution in the ANN simulation and to reduce the challenge of numerical instability in the process of adjusting weights, the inputs to the model were normalized and scaled into the numeric range [-1,1].

The *tangent-sigmoid* transfer function was selected that is compatible with the normalization range of input variables since it is known to show the least sensitivity to the numerical method for computing the differentials. Moreover, the adaptive characteristic of *tangent-sigmoid* facilitates the operations over the entire range of inputs, which yields significantly higher slope of the transfer function curve under small input magnitudes and substantially lower slope under higher input magnitudes. This improves the rate of the learning performance of the network. The linear activation functions were used in the output layer.

Backpropagation (BP) training algorithm employs the iterative-based gradient descent optimization technique to minimize the mean square error between the actual and predicted output. In this manner, the synaptic weights are updated in an iterative manner until the predefined goal of realizing either 0 or a minimum of MSE within the preset 1000 iterations is attained. The damped least-square optimization method was employed to yield rapid convergence during the training phase by updating the weights and biases. The reliability of any neural representation is generally verified using different statistical indices for quantifying the closeness of the actual and predicted outputs. In this study, the mean square error (MSE) between the predicted and actual feedback gains of the optimal controller and the coefficient of determination (R^2) are adopted to evaluate performance of the proposed NN.

IV. Results and Discussion

The neural network system herein accommodates 2 inputs (i.e., the states of the system) and estimates 2 outputs referring to the feedback gains of the optimal controller. The NN representation includes a single hidden layer with varying neurons. The weights were randomly scaled into the interval [-1 1] while training and testing data sets were obtained by employing independent and identically distributed uniform sequence over [-1,1] for 10000 data points. Using a trial-error approach in order to identify the least MSE value, the optimal number of neurons in the single hidden layer was obtained at 25 considering the system nonlinearities and the considerable size of data. To ensure the reliable learning speed of the neuro-optimal controller, the learning rate and momentum factors were employed. The learning rate regulates the intensity of decreasing the error iteratively and applies either a greater or smaller magnitude of modification to the preceding weight [28]. The neural network can potentially be trained rapidly in case the learning factor is considered large at the cost of losing the accuracy and generalization particularly when there is a large variableness in the input set. Therefore, setting the learning rate to a large value is improper and counterproductive to learning. Consequently, it is advised to set the factor to a small value and edge it upward where the learning rate seems to be at a low pace [33]. Momentum on the other side performs as a low-pass filter to settle sudden changes in the training procedure by allowing a variation to the weights in order to persevere for a number of adjustment cycles. If the momentum factor is set to a nonzero value, then progressively greater persistence of previous adjustments is acceptable in changing the current adjustment. The optimal values for the learning rate and momentum were obtained at 0.4 and 0.7 through a trial and error examination.

Fig. 3 shows the results of the training, validation, and testing phases of the proposed neural network representation to estimate the feedback gains of the system in terms of the coefficient of determination. The error convergence toward zero at the desired rate and minimal complexity in NN can be appreciated from Fig. 3. It is further inferred that the estimated feedbacks have converged toward the unity slope line with a very small bias magnitude invariably for all of the three phases. It is further perceived that the range of feedback gains cover both the positive and negative values depending on the state the system.

Fig. 4 presents the MSE curves in the logarithmic scale for both the training and testing data sets. Fig. 4 is suggestive that most of the NN learning was progressively continued until it reached the maximum of 1000 iterations; however, MSE reduction for the testing phase was finalized within the iterations less than 40. The modeling performance for the testing phase indicates that the proposed neural estimator can predict the desired feedback gain adaptively to follow the desired trajectories given any disturbance or uncertainties in the system. The lowest MSE pertaining to the outperforming representation was obtained at 9.92e-10, which also equals to the best validation performance.

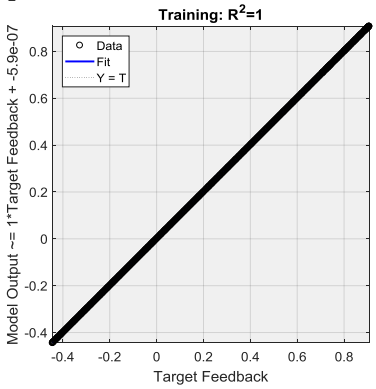

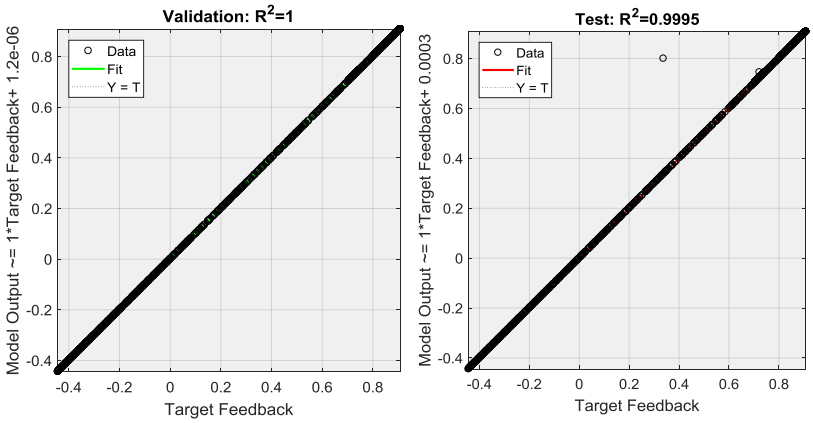

Fig. 3. The coefficient of determination of the NN estimator for the three phases of training, testing and validation, respectively.

Furthermore, the augmented neural training, testing, and validation outputs compared to the actual feedback gains reveal that there was a very small error during all of the number of data indices although there were very negligible variations in the error estimation for feedback matrix (Fig. 5).

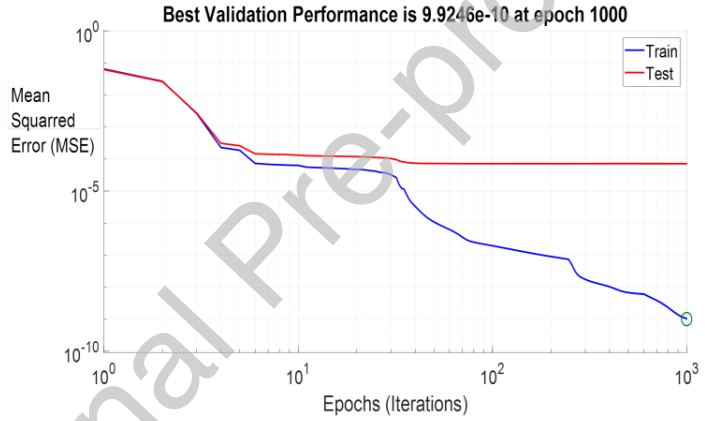

Fig. 4. The variations in MSE for the training and testing phases in the logarithmic scale

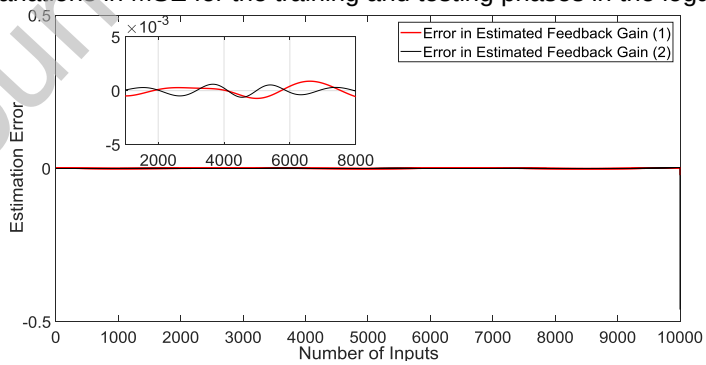

Fig. 5. The instantaneous modeling error

The vehicle forward speed was initially set at 110 km/h, while the road friction coefficient was considered at 0.6 in order to limit the upper bound of the desired yaw rate. Two sinusoidal steering maneuvers were utilized characterized by 0.75 Hz and 1.25 Hz of frequency. In the first scenario, a 0.75 Hz open-loop sinusoidal steering maneuver for the duration of 2 seconds was applied after a lapse time of 1.25s. In the second scenario, a 1.25 Hz sinusoidal steering maneuver was utilized applied for duration of 4s including laps time after and before the start of sinusoidal input. Fig. 6 shows the vehicle response to the first sinusoidal input which indeed acts as the system disturbance. The vehicle response is synthesized in

terms of the yaw rate and the side-slip angle to follow the desired trajectories as shown in Fig. 6. It can be distinguished that proposed controller compensates the vehicle to follows the desired yaw rate and side-slip angle rapidly. The controller input generated by the proposed nonlinear neuro-optimal controller is shown in Fig. 6. Fig. 7 illustrates the yaw rate and vehicle side-slip angle responses in step steer maneuver condition for uncontrolled system, conventional SMC method according to [34], and the proposed AORC to track the desired trajectories. It can be seen that since the tires exceeding the saturation region (*i.e.* $a_{y\,max} = 0.7\,g$), the conventional vehicle cannot generate enough lateral forces for cornering, SMC converges toward the desired trajectory and the uncontrolled system diverges from the desired responses. In terms of the controller input, the proposed controller is suggestive of considerably lower magnitude which can be attributed to the optimization of the cost function related to the controller. Fig. 8 presents the desired and closed-loop yaw rate and side-slip angle of the vehicle model using the conventional SMC, uncontrolled method, and proposed controller with the controller input under the higher frequency steering input representative of double lane change maneuver according to [34]. It can be seen that the uncontrolled system diverges from the desired trajectory and the conventional SMC converges to the desired trajectory with an offset when compared to the proposed AORC method.

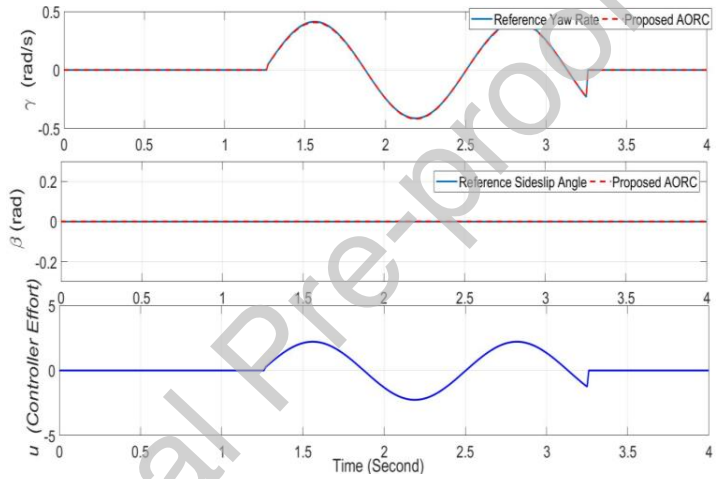

Fig. 6. The vehicle response to the low-frequency sinusoidal input using the proposed closed-loop controller

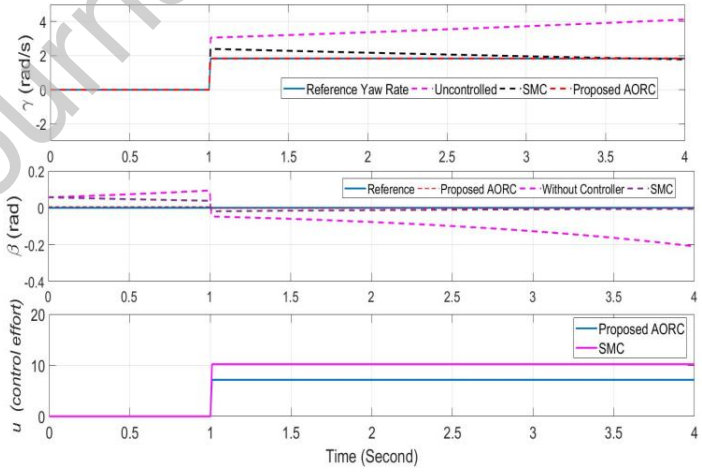

Fig. 7. Yaw rate and vehicle side-slip angle responses in step steer maneuver condition for different controlling methods

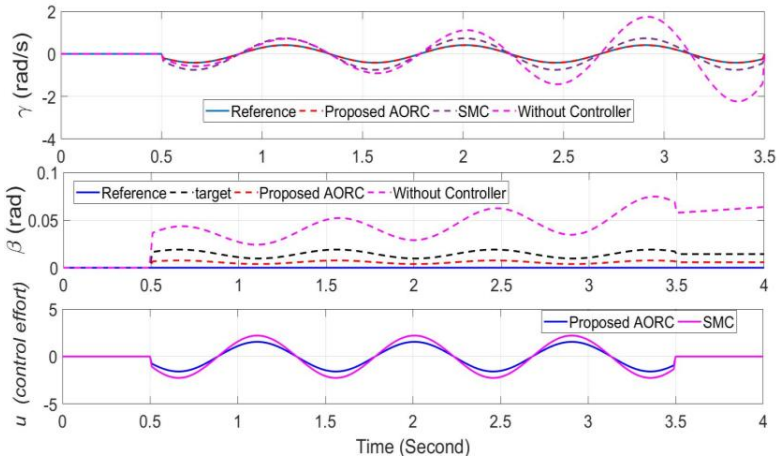

Fig. 8. The vehicle response to the high-frequency sinusoidal input using the proposed closed-loop controller

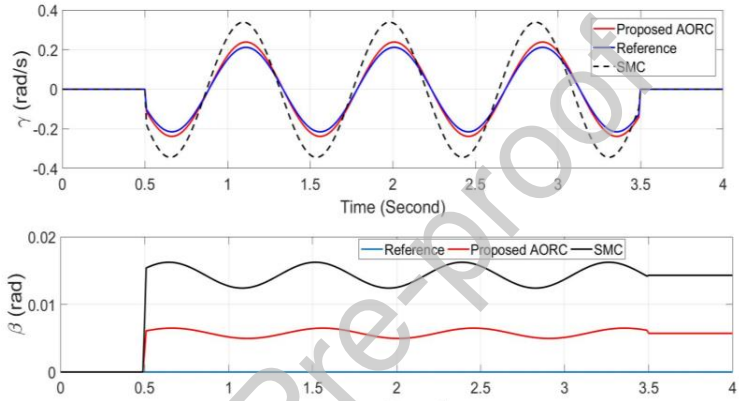

Fig. 9. The vehicle response to the parametric uncertainty and bounded external disturbance

The effectiveness of the proposed controller to withstand the parametric uncertainty and bounded external disturbance according to the proof provided from (23) to (36) is presented in Fig. 9 while mass, cornering stiffness of tires and mass moment of inertia are perturbed by 20% about their nominal values and a limited external disturbance due to the wind force is considered. It can be seen that although both of the controllers remain in the stable region, the proposed AORC keeps tracking of the desired yaw rate and side-slip angle in a more effective manner. Fig. 10 compares the open-loop and closed-loop accelerations during the high-frequency sinusoidal front steering angle variations. It can be perceived that the lateral acceleration corresponding to the closed-loop acceleration is considerably less than the open-loop vehicle response, which is achieved through the decrease of the closed-loop controller yaw rate response. This is critically significant particularly during severe maneuvers at high speeds to guarantee the lateral stability and handling. Furthermore, the capacity of the obstacle avoiding and path following the vehicle at high speed can also improve drastically.

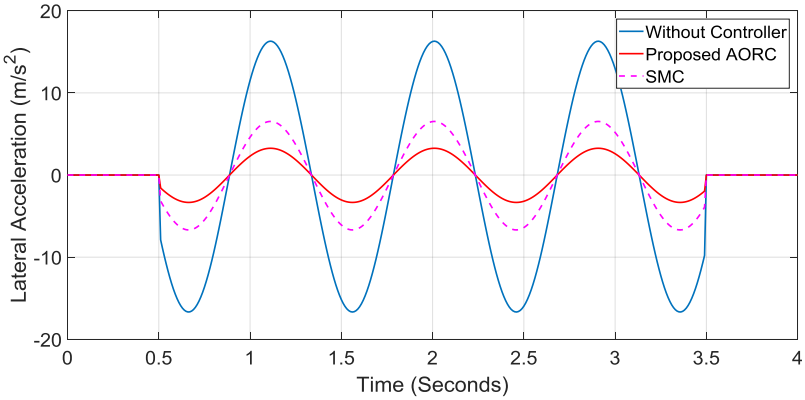

Fig. 10. The open-loop and closed-loop accelerations during the high-frequency sinusoidal front steering angle

V. CONCLUSIONS

In this paper, an optimal robust controller coupled to a damped least-square Backpropagation training of neural networks (NN) was proposed to enhance the vehicle lateral dynamics stability and handling performance. To this end, a four-wheel active steering (4WAS) vehicle model was employed to control the yaw rate and side-slip angle of the vehicle to track the desired responses. The nonlinearities and uncertainties in the vehicle model, together with the effect of external disturbance were handled using the developed FFBPNN algorithm while the corresponding optimal feedback gains for a wide range of operating conditions were generated. The stability of the proposed controller was proved using a Lyapunov stability method and three maneuvering conditions, including step steering and double lane change, were employed to verify the effectiveness of the proposed controller with and without the presence of parametric uncertainties and external disturbance. The results of the proposed controller were also compared to classical SMC and open-loop system, and it is concluded that the proposed control schema can substantially enhance the handling and stability performances of the vehicle for a broad range of operating conditions in a robust manner. Although this algorithm provides a satisfactory performance when compared to the benchmarking methods, the effect of actuator saturation and time-delay on the performance of the proposed controller will be further studied in future works.

Declaration of interests

The authors declare that they have no known competing financial interests or personal relationships that could have appeared to influence the work reported in this paper.

REFERENCES

[1] Hu, C., Wang, Z., Taghavifar, H., Na, J., Qin, Y., Guo, J., & Wei, C. (2019). MME-EKF-Based Path-Tracking Control of Autonomous Vehicles Considering Input Saturation. *IEEE Transactions on Vehicular Technology*, 68(6):5246-5259.

[2] Wei, C., Romano, R., Merat, N., Wang, Y., Hu, C., Taghavifar, H., & Boer, E. R. (2019). Risk-based autonomous vehicle motion control with considering human driver's behaviour. *Transportation Research Part C: Emerging Technologies*, *107*, 1-14.

[3] Li, B., Rakheja, S., & Feng, Y. (2016). Enhancement of vehicle stability through integration of direct yaw moment and active rear steering. *Proceedings of the Institution of Mechanical Engineers, Part D: Journal of Automobile Engineering*, *230*(6), 830-840.

[4] Chuan Hu, Hongbo Gao, Jinghua Guo, Hamid Taghavifar, Chongfeng Wei, and Yechen Qin, and Jing Na, RISE-Based Integrated Lane-Keeping and Roll Control of Autonomous Ground Vehicles with Asymptotic Prescribed Performance, *IEEE Transactions on Systems, Man, and Cybernetics: Systems*, 2019.

[5] Di Cairano, S., Tseng, H. E., Bernardini, D., & Bemporad, A. (2013). Vehicle yaw stability control by coordinated active front steering and differential braking in the tire side-slip angles domain. IEEE Transactions on Control Systems Technology, 21(4), 1236-1248.

[6] Zhao, W., Qin, X., & Wang, C. (2018). Yaw and lateral stability control of Automotive four-wheel steer-by-wire system. *IEEE/ASME Transactions on Mechatronics*.
[7] Rajamani, R. (2011). Vehicle dynamics and control. Springer Science & Business Media.
[8] Yu, Shuyou, Jing Wang, Yan Wang, and Hong Chen. "Disturbance observer based control for four wheel steering vehicles with model reference." *IEEE/CAA Journal of Automatica Sinica* (2016).
[9] Jin, X., Yu, Z., Yin, G., & Wang, J. (2017). Improving Vehicle Handling Stability Based on Combined AFS and DYC System via Robust Takagi-Sugeno Fuzzy Control. *IEEE Transactions on Intelligent Transportation Systems*.
[10] Ni, J., Hu, J., & Xiang, C. (2017). Envelope control for four-wheel independently actuated autonomous ground vehicle through AFS/DYC integrated control. *IEEE Transactions on Vehicular Technology*, *66*(11), 9712-9726.
[11] Zhao, J., Wong, P. K., Ma, X., & Xie, Z. (2017). Chassis integrated control for active suspension, active front steering and direct yaw moment systems using hierarchical strategy. *Vehicle System Dynamics*, 55(1), 72-103.
[12] Zhang, H., & Wang, J. (2016). Vehicle lateral dynamics control through AFS/DYC and robust gain-scheduling approach. *IEEE Transactions on Vehicular Technology*, *65*(1), 489-494.
[13] Zhang, H., Zhang, X., & Wang, J. (2014). Robust gain-scheduling energy-to-peak control of vehicle lateral dynamics stabilisation. *Vehicle System Dynamics*, *52*(3), 309-340.
[14] Li, L., Lu, Y., Wang, R., & Chen, J. (2017). A three-dimensional dynamics control framework of vehicle lateral stability and rollover prevention via active braking with MPC. *IEEE Transactions on Industrial Electronics*, *64*(4), 3389-3401.
[15] Song, Pan, Masayoshi Tomizuka, and Changfu Zong. "A novel integrated chassis controller for full drive-by-wire vehicles." Vehicle System Dynamics 53, no. 2 (2015): 215-236.
[16] Abe M and Mokhiamar O. An integration of vehicle motion controls for full drive-by-wire vehicle. Proc IMechE Part K: J Multi-body Dynamics 2007; 221: 116–127.
[17] Zhuang, D-J., F. Yu, and Y. Lin. "Evaluation of a vehicle directional control with a fractional order PD μ controller." International Journal of Automotive Technology 9, no. 6 (2008): 679-685.
[18] Hou, Yuming, Jie Zhang, Yunqing Zhang, and Liping Chen. "Integrated chassis control using ANFIS." In Automation and Logistics, 2008. ICAL 2008. IEEE International Conference on, pp. 1625-1630. IEEE, 2008.
[19] Li, B., and F. Yu. "Design of a vehicle lateral stability control system via a fuzzy logic control approach." *Proceedings of the Institution of Mechanical Engineers, Part D: Journal of Automobile Engineering* 224.3 (2010): 313-326.
[20] Song, J. (2012). Integrated control of brake pressure and rear-wheel steering to improve lateral stability with fuzzy logic. *International Journal of Automotive Technology*, *13*(4), 563-570.
[21] Chen, C., Modares, H., Xie, K., Lewis, F. L., Wan, Y., & Xie, S. (2019). Reinforcement learning-based adaptive optimal exponential tracking control of linear systems with unknown dynamics. *IEEE Transactions on Automatic Control*.
[22] Chen, C., Lewis, F. L., Xie, S., Modares, H., Liu, Z., Zuo, S., & Davoudi, A. (2019). Resilient adaptive and H∞ controls of multi-agent systems under sensor and actuator faults. Automatica, 102, 19-26.
[23] Chen, C., Liu, Z., Zhang, Y., & Chen, C. P. (2015). Adaptive control of robotic systems with unknown actuator nonlinearities and control directions. *Nonlinear Dynamics*, *81*(3), 1289-1300.
[24] Li, B., & Yu, F. (2009, June). Optimal model following control of four-wheel active steering vehicle. In *Information and Automation, 2009. ICIA'09. International Conference on* (pp. 881-886). IEEE.
[25] Mohammadzadeh, A., Kaynak, O., & Teshnehlab, M. (2014). Two-mode indirect adaptive control approach for the synchronization of uncertain chaotic systems by the use of a hierarchical interval type-2 fuzzy neural network. *IEEE Transactions on Fuzzy Systems*, 22(5), 1301-1312.
[26] Esmailzadeh, E., Goodarzi, A., & Vossoughi, G. R. (2003). Optimal yaw moment control law for improved vehicle handling. Mechatronics, 13(7), 659-675.
[27] Chai, R., Savvaris, A., Tsourdos, A., Chai, S., & Xia, Y. (2017). Trajectory optimization of space maneuver vehicle using a hybrid optimal control solver. IEEE transactions on cybernetics, 49(2), 467-480.
[28] Chai, R., Tsourdos, A., Savvaris, A., Chai, S., & Xia, Y. (2018). Two-stage trajectory optimization for autonomous ground vehicles parking maneuver. IEEE Transactions on Industrial Informatics.
[29] Kiencke U and Nielsen L. Automotive control systems: for engine, driveline and vehicle. Berlin: Springer, 2000.
[30] Savaresi, S. M., & Tanelli, M. (2010). Control-oriented Models of Braking Dynamics. In Active Braking Control Systems Design for Vehicles (pp. 17-52). Springer London.
[31] Du, H., Li, W., & Zhang, N. (2012). Integrated seat and suspension control for a quarter car with driver model. *IEEE transactions on vehicular technology*, 61(9), 3893-3908.
[32] Neural Network Design (2nd Edition) Martin T. Hagan, Howard B. Demuth, Mark H. Beale, Orlando De Jesus ISBN-10: 0-9717321-1-6 ISBN-13: 978-0-9717321-1-7.
[33] Taghavifar, H., & Mardani, A. (2014). Use of artificial neural networks for estimation of agricultural wheel traction force in soil bin. *Neural* Computing and Applications, 24(6), 1249-1258.
[34] Li D, Du S and Yu F. Integrated vehicle chassis control based on direct yaw moment, active steering and active stabilizer. Veh System Dynamics 2008; 46(1): 341–351.

Hamid Taghavifar is currently an Assistant Professor with the School of Mechanical, Aerospace and Automotive Engineering, Coventry University, UK. Formerly, he was a Vehicle Ride and Handling Engineer at Fiat Chrysler ARDC, after working as a Horizon Postdoctoral Fellow at CONCAVE Research Center, Concordia University in Canada. His research focuses on automated driving, control of autonomous systems (adaptive, nonlinear, and intelligent), robotics and artificial intelligence, where he has contributed over 50 peer-reviewed papers, a book, and 2 Iranian registered patents. He serves as the Editor-in-Chief of the Journal of Advances in Vehicle Engineering, Editor for Int. J. of Vehicle Systems Modelling and Testing and Int. J. of Vehicle Information and Communication Systems.

Chuan Hu is currently a Postdoctoral Fellow in the Department of Mechanical Engineering, University of Texas at Austin, Austin, USA. He was a Postdoctoral Fellow in the Department of Systems Design Engineering, University of Waterloo, Waterloo, Canada from July 2017 to July 2018. He received the B.E. degree in vehicle engineering from Tsinghua University, Beijing, China, in 2010, the M.E. degree in vehicle operation engineering from the China Academy of Railway Sciences, Beijing, in 2013, and the Ph.D. degree in Mechanical Engineering, McMaster University, Hamilton, Canada in 2017. His research interest includes vehicle system dynamics and control, motion control and estimation of autonomous vehicles, mechatronics, robust and adaptive control.

Leyla Taghavifar obtained her B.Sc. and M.Sc. degrees in Electrical Engineering from Tabriz University, and IAU of Tehran, Iran, in 2009 and 2013, respectively. Her research interests include signal processing and synchronization, telecommunications, cellular networks and artificial intelligence.

Yechen Qin received the B.Sc. degree and Ph.D. degree in Mechanical Engineering from Beijing Institute of Technology, P.R. China in 2010 and 2016, respectively. He is currently working as associate professor in Beijing Institute of Technology, P.R. China. From 2013 to 2014, he was studied in Texas A&M University, US as a visiting Ph.D. student. He has also worked in Beijing Institue of Technology and University of Waterloo as postdoctoral research fellow and visiting scholar. His research interests include vehicle dynamics control and road estimation.

Jing Na received the B.Eng. and Ph.D. degrees in control engineering from the School of Automation, Beijing Institute of Technology, Beijing, China, in 2004 and 2010, respectively. From 2011 to 2013, he was a Monaco/ITER Post-Doctoral Fellow with ITER Organization, Saint-Paul-l\`es-Durance, France. From 2015 to 2017, he was a Marie Curie Intra-European Fellow with the Department of Mechanical Engineering, University of Bristol, Bristol, U.K. Since 2010, he has been with the Faculty of Mechanical and Electrical Engineering, Kunming University of Science and Technology, Kunming, China, where he became a Full Professor in 2013. He has co-authored one monograph published in Elsevier and authored or co-authored over 100 international journal and conference papers. His current research interests include intelligent control, adaptive parameter estimation, nonlinear control and applications for robotics, vehicle systems, and wave energy convertor. Dr. Na was a recipient of the Marie Curie Fellowship from EU, the Best Application Paper Award of the 3rd IFAC International Conference on Intelligent Control and Automation Science in 2013, and the 2017 Hsue-Shen Tsien Paper Award. He is currently an Associate Editor of Neurocomputing and has served as the IPC Chair of ICMIC in 2017.

Chongfeng Wei obtained the B.Sc. degree in computational and applied mathematics and the M.Sc. degree in vehicle engineering from Southwest Jiaotong University, Chendu, China, in 2009 and 2011, respectively, and the Ph.D. degree in mechanical engineering from the University of Birmingham in 2015. After two and a half years postdoctoral research period, he joined the School of Mechanical Engineering at Shanghai Jiao Tong University as an Assistant Professor (tenure-track). He then moved to the institute of Transport Studies at University of Leeds as a research fellow in 2018. His current research focuses on Humanlike autonomous vehicle control and collision avoidance